The geology and petrochemistry of the Mashikiri Formation along the Olifants River Section, Kruger National Park, South Africa.

H. de Bruiyn, A.E. Schoch, D.S. Fairwood and W.A. van der Westhuizen
Department of Geology, University of the Free State, P.O. Box 339, Bloemfontein 9300, South Africa
e-mail: dbruiynh.sci@mail.uovs.ac.za

ABSTRACT

The volcaniclastic sediments and nephelinite lavas of the Mashikiri Formation, Lebombo Group, have been well documented in the Pafuri region and in the Sabi region, Zimbabwe. The well-exposed section along the Olifants River in the Kruger National Park provides cogent additional information. The Shishwayini Beds at the base of the succession represents volcaniclastic deposits on the Tshipise Sandstone Member of the Clarens Formation. The rest of the Mashikiri Formation in the Olifants River section is nephelinite in which nepheline is accompanied by olivine, clinopyroxene, devitrified glass, katophorite and opaque oxides. Chemical modelling shows that the nephelinites were derived by partial melting of mantle peridotite enriched in incompatible trace elements and by subsequent fractionation of pyroxene and olivine. Crustal contamination did not play a significant role in derived magma composition. The Olifants River section defines a third source of undersaturated parent magma distinct from the two sources previously identified from outcrops to the north by other authors.

Introduction

The break-up of Gondwana commenced with silica-undersaturated volcanicity (Cox *et al.*, 1967; Rhodes and Krohn, 1972; Cox, 1978a; b; 1980; Eales *et al.*, 1984; Wilson, 1989; Coffin and Eldholm, 1994; White and McKenzie, 1995; Duncan *et al.*, 1997). The monoclinal structure of the Lebombo provides an ideal profile through the volcanic succession. In the Olifants River section the basal sequence is represented by nephelinites and volcaniclastics (Figure 1). Other nephelinite outcrops occur in separated areas to the north. In his excellent study of the nephelinites of the Pafuri and Sabi (Zimbabwe) regions, Bristow (1980) correlates the rocks with those of the Olifants River occurrence. Cleverly and Bristow (1979) proposed the term Mashikiri Formation to collectively group the undersaturated alkali rocks from the three different outcrop regions. The aim of the present study is to provide a coherent set of geochemical analyses and petrographic descriptions for the characterisation of the Olifants River profile.

Regional Geology and Tectonic Setting

The Lebombo monocline is a major geological feature, extending northwards from Natal, South Africa over 750km through Swaziland to Zimbabwe. The rocks under discussion form part of the Lebombo Group (Schutte, 1986) of the Mesozoic Karoo Supergroup. In the study area the volcanic rocks of the Lebombo Group have extruded upon a relatively thin layer of Karoo sediments that is correlated with the Clarens Formation of the Karoo basin (Schutte, 1986). At the western edge of the monocline, the Mesozoic rocks rest mainly on granitic basement of the Kaapvaal Craton (Bristow, 1980) and to the east, in Mozambique, the Lebombo Group volcanics are overstepped by marine sediments of Cretaceous age (Eales *et al.*, 1984). In the Kruger National Park (KNP) the relevant basement comprises several units. These are (i) in the south: Swazian rocks of the Nelspruit Granite Suite (~3.2 Ga, Barton *et al.*, 1986), tonalitic and trondhjemitic gneisses and the Orpen Gneiss, (ii) in the north: Swazian rocks of the Goudplaats Gneiss (>~3.5 Ga; Barton *et al.*, 1986) and the Makhutswi Gneiss (Jantsky, 1980). The Goudplaats Gneiss contains xenoliths that are similar to the oldest exposed rocks in the KNP, representing the Murchison and Sutherland greenstone belts (Barton *et al.*, 1986). The granitic basement rocks to the west of the study area are intruded by small bodies of Timbavati Gabbro dated at ~1.45 Ga (Barton *et al.*, 1986).

Field Relations

Rocks of the Lebombo Group are exposed along a 50 km stretch of the Olifants River in South Africa. The detailed field relations of the Mashikiri Formation along the Olifants River section are shown in Figure 2. All mappable units in the profile are represented by very distinctive rocks (Table 1).

The lowermost rocks of Karoo age in the study area are sandstones, correlated with the Tshipise Sandstone Member of the Clarens Formation (Schutte, 1986; Bristow and Venter, 1986). The sandstones are generally massive, displaying dune cross-bedding and structures. Carbonate nodules and concretions also occur and ubiquitous calcite veining has an average trend of 020. Iron oxide staining and iron-manganese dendrites are conspicuous on some surfaces.

A thin, locally-developed layer (~130cm; the Shishwayini Beds, Table 1) of reworked volcanic material (Figures 3 and 4) represents the lowermost volcanic rocks. These volcaniclastics rest unconformably upon the Clarens Formation.

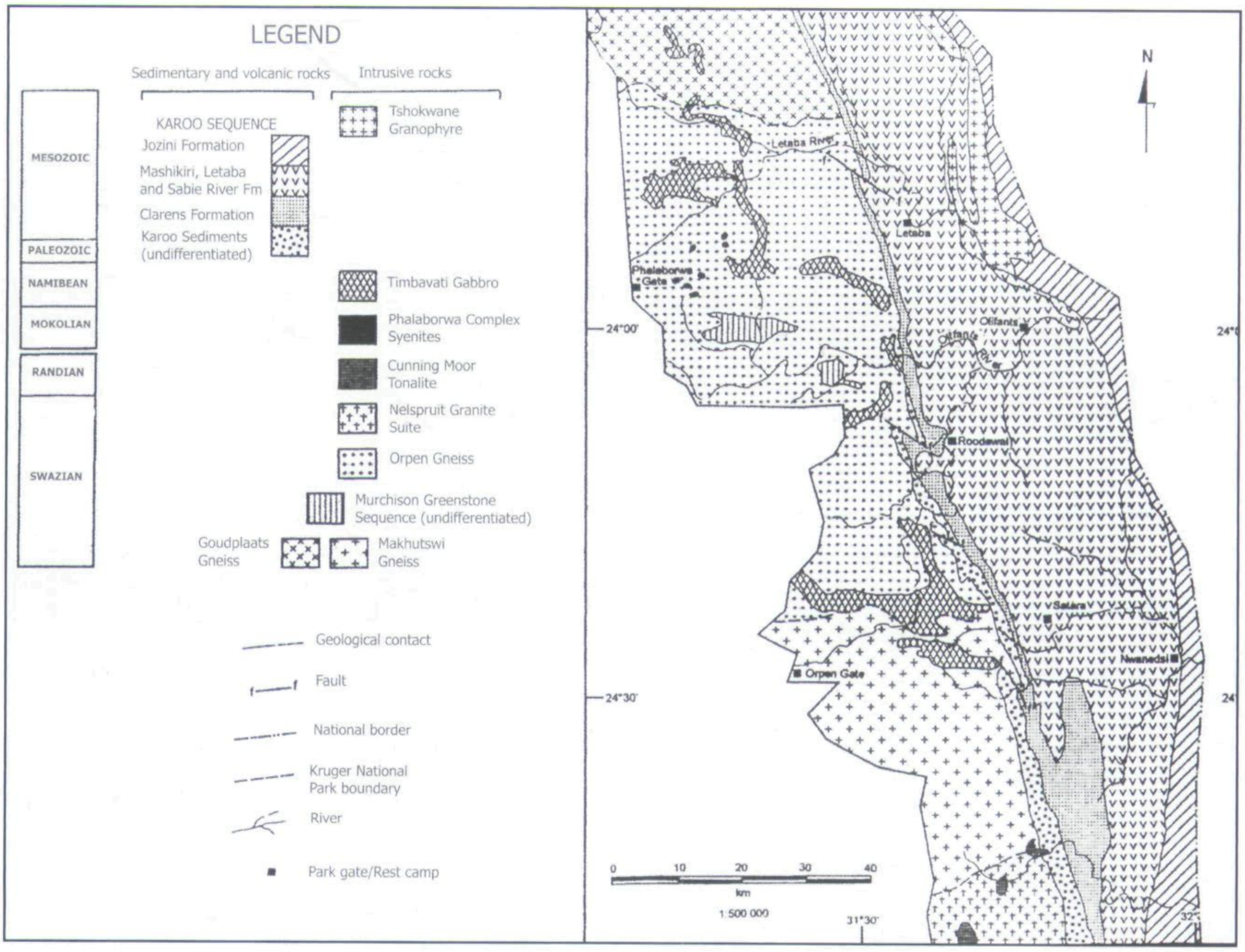

Figure 1. Geological locality map showing the distribution of the Mashikiri and related formations (v ornament) along the central part of the Kruger National Park (adapted from Schutte, 1986). Details of the traverse along part of the Olifants River are supplied in Figure 2.

The volcaniclastics are macroscopically distinctive (deep red-brown colour and conspicuous bedding planes) with a variety of sedimentary structures. The latter includes planar and trough cross-bedding, as well as erosional channel features and de-watering disruptions (lower middle, Figure 3). The Shishwayini Beds can be subdivided into five laterally persistent units (Figure 5). The thickness and grain-size of individual units are highly variable.

A thick sequence of black to dark grey nephelinite lavas (~300m) overlies the volcaniclastics in the study region and has an average dip of 10° to the west. The rocks possess a distinctive phenocryst assemblage and texture with vesicles and large amygdales filled by quartz and calcite. The lower contact with the volcaniclastics is irregular. Extrusion of the lava caused disruption of the subjacent sediment (Figure 4). A highly brecciated zone that reaches a thickness of 50cm occurs

Table 1. Determined thicknesses of the Lebombo Group in the Olifants River section (stratigraphic subdivision according to Cleverly and Bristow, 1979).

Formation	Beds	Thickness	Best Age	Lithologies
Jozini		4.2km	177±6 Ma (a)	Rhyolite ash-flows with interbedded basalts
Sabi River		5.6km	178 Ma (b)	Low-Mg basalts
	Upper Olifants			Rhyolite lava
	Lower Olifants			Rhyolite lava
Letaba		1.3km	177±9 Ma (b)	Picro-basalts
Mashikiri		~300m	178 Ma (b)	Nephelinites
	Shishwayini	~130cm		Volcanoclastics
		Unconformity		
Clarens		Unknown	~210 Ma (c)	Aeolian sandstone
		Unconformity		
Kaapvaal Basement			pre 3200 Ma (d)	Granitic gneiss

a) Allsopp *et al.* (1984) b) Fitch and Miller (1984) c) Henthorn (1981) d) Barton *et al.* (1984)

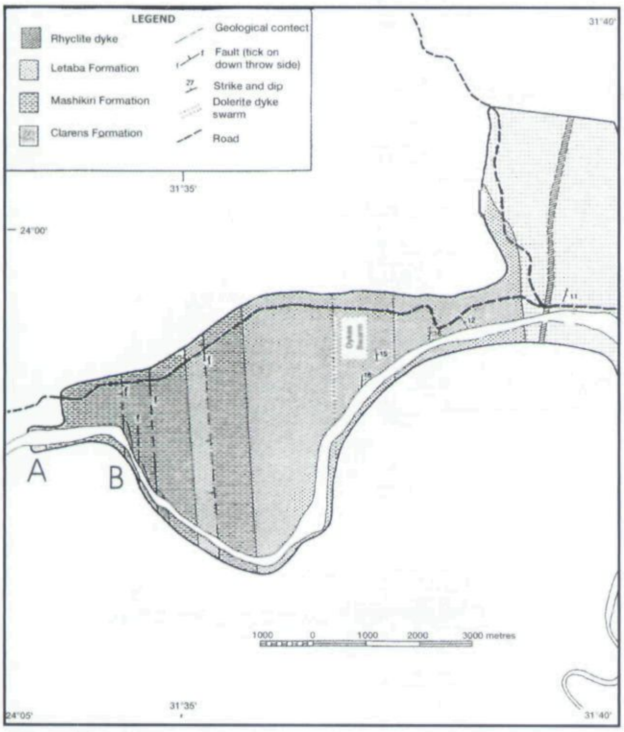

Figure 2. Geological outcrop map of the Mashikiri Formation exposed along the Olifants River. The regional geological context is supplied in Figure 1. The numbered localities are referred to in the text

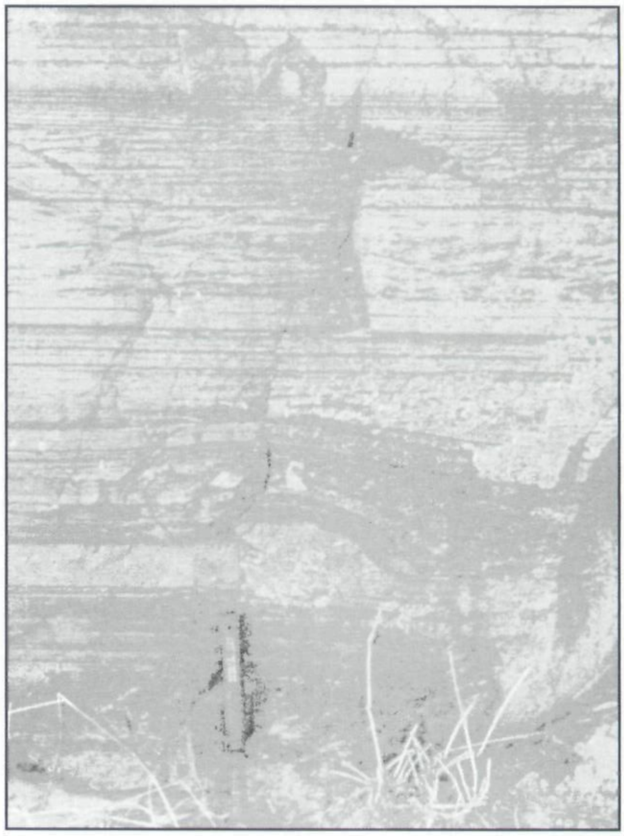

Figure 3. Volcaniclastic sediments at the base of the Mashikiri Formation (Shishwayini Beds), Olifants River. Looking east, locality 1, Figure 2. The head of the geological hammer is resting on Clarens sandstone.

Figure 4. Details of the contact between the volcaniclastic sediments (Shishwayini Beds, pseudo-layered material in the bottom half of the photograph) at the base of the Mashikiri Formation with overlying nephelinite lava flows. The leucocratic zone to the left of the pick end of the geological hammer represents brecciation caused by phreatic activity. Looking east, locality 2, Figure 2.

at the base of the lowest nephelinite flow. Large vesicles (0.5mm to 2cm) are developed in this zone. The brecciated and incorporated sediments are interpreted to indicate eruption onto wet, unconsolidated material, with attendant phreatic activity.

In the basal nephelinite flow, amygdales gradually become less upwards and vesicles smaller and more spherical. Discernible flow-banding is present immediately above the breccia zone in localised patches. About 50cm above the base of the first flow, large black pyroxene and small olivine phenocrysts appear. However, it is only higher up in the sequence that the characteristic texture becomes conspicuous (pyroxene clusters, up to 5cm in diameter, accompanied by euhedral olivine). The exposed thickness of the Mashikiri Formation in the study region is almost doubled by numerous normal faults (Figure 2). The displacement of each fault is of the order of a few metres, with an average strike of 025.

Petrography and Mineralogy

Olivine and clinopyroxene phenocrysts are present in nearly all of the nephelinite lava flows. Grain size varies widely from devitrified hypohyaline (olivine phyric) to holocrystalline porphyritic (pyroxene phenocrysts). Phenocrysts of opaque oxides are rare. The optically distinguishable groundmass in fine-grained lavas consists of pyroxene needles, nepheline and opaque oxides. Large patches of brown devitrified glass are common, especially in flows at the base of the succession. Coarser grained matrix comprises altered nepheline, a colourless isotropic mineral and clay minerals. Rare patches of late crystallisation with nepheline, analcite and K-feldspar were first noted by Bristow (1980).

Pyroxene in the nephelinites is highly variable in terms of modal per cent (10 to 35), crystal morphology (euhedral to subhedral), crystal size (0.5mm to 8cm) and

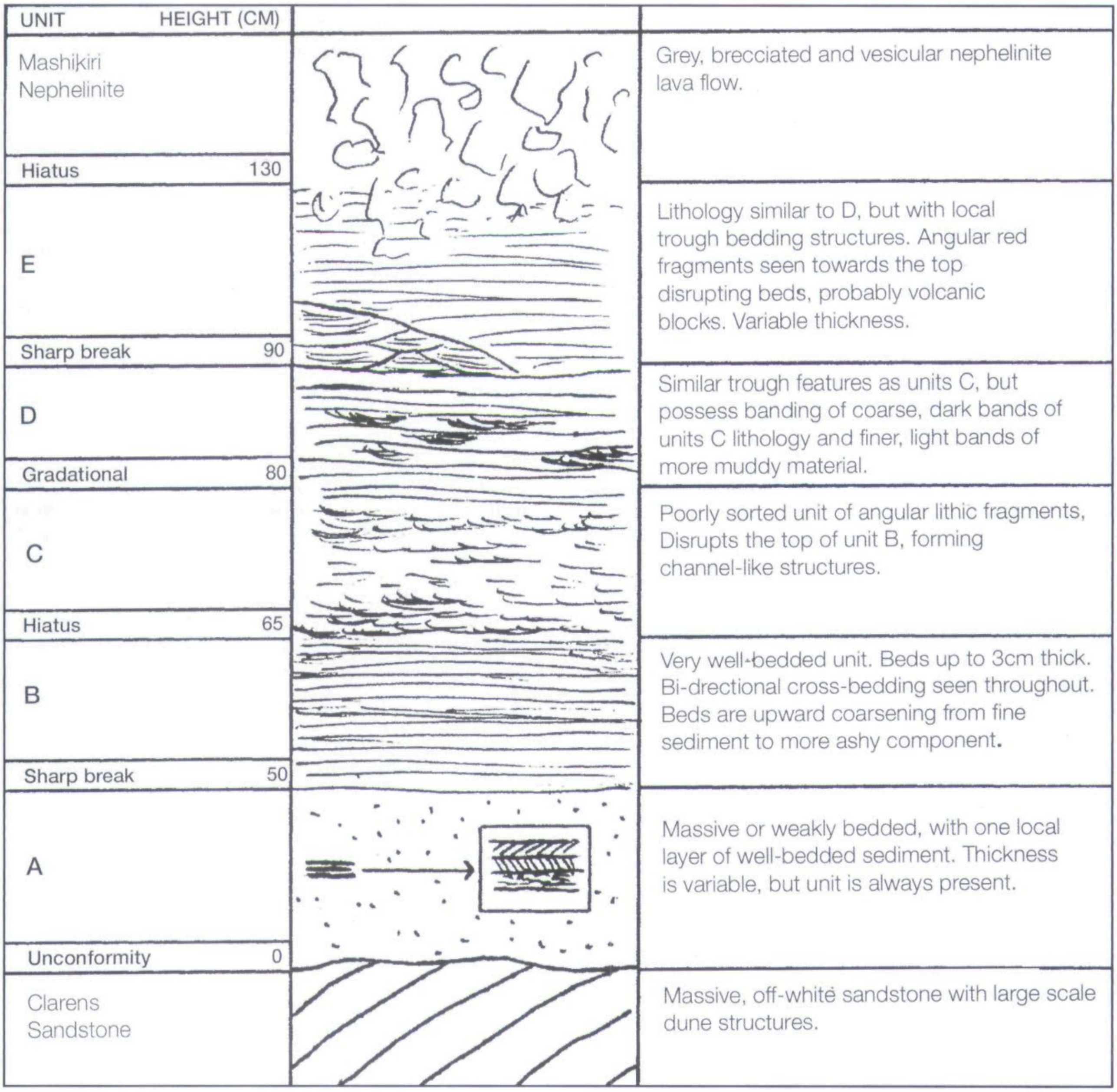

Figure 5. Structural details of the Shishwayini Beds of the Mashikiri Formation.

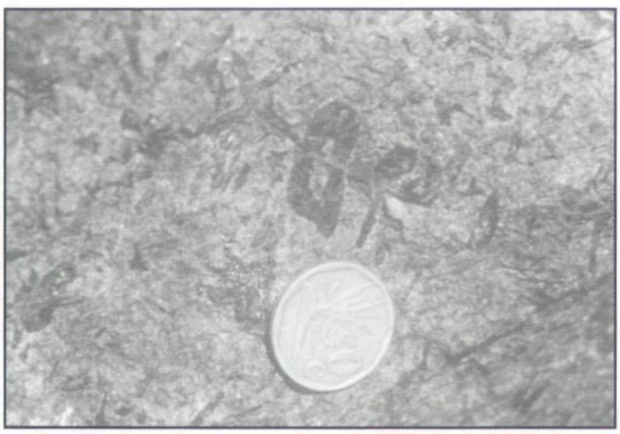

Figure 6. Glomeroporphyritic texture in nephelinite (note the "birds-foot" cluster above right of the coin).

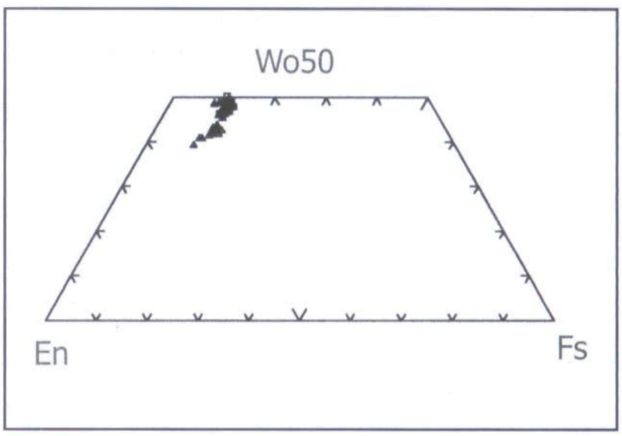

Figure 7. Analytic data for augitic phenocryst pyroxene in the nephelinite of the Mashikiri Formation, projected on the pyroxene trapezium.

Table 2. Mean pyroxene compositions and structural formulae (to 6 oxygen atoms) from the nephelinites of the Mashikiri Formation.

		Augite		Jadeite
	2-cpx	36-cpx	238-cpx	2-cpx
SiO_2	51.57	50.90	50.21	49.81
TiO_2	0.66	0.79	0.90	0.00
Al_2O_3	4.03	3.45	3.69	28.79
Cr_2O_3	0.16	0.06	0.04	0.01
FeO	6.66	6.73	6.99	0.06
MnO	0.10	0.10	0.10	0.02
MgO	14.99	13.84	13.54	0.01
CaO	19.41	22.16	22.49	0.23
Na_2O	1.09	1.13	1.04	20.48
K_2O	0.01	0.01	0.01	0.01
Total	98.68	99.17	99.01	99.42
Si	1.92	1.90	1.89	1.75
Al^{iv}	0.08	0.10	0.11	0.25
T-site	2.00	2.00	2.00	2.00
Al^{vi}	0.10	0.06	0.05	0.94
Ti	0.02	0.02	0.03	0.00
Fe	0.21	0.21	0.22	0.00
Ng	0.83	0.77	0.76	0.00
Ca	0.77	0.89	0.91	0.01
Na	0.08	0.08	0.05	1.40
M1,M2	2.01	2.04	2.04	2.35
En	46	41	40	
Fs	11	11	12	
Wo	43	47	48	

chemical composition (Table 2). Three generations of clinopyroxene phenocrysts are represented by zoned megacrysts, partially resorbed cores, and unzoned small subhedral phenocrysts with no evidence of zoning or twinning. The megacrysts tend to form glomeroporphyritic "birdsfoot" textures (Figure 6), frequently in association with olivine. The colour ranges from black to light brown. Complex concentric zoning, as well as twinning is common in some of the largest crystals. Chadacrysts of opaque oxides occur in peripheral zones.

The large range in mineral chemistry is clearly demonstrated by representative pyroxene analyses (Table 2, $En_{40}Wo_{48}Fs_{12}$ to $En_{46}Wo_{43}Fs_{11}$ and jadeite) and exhibits a trend of Mg-Ca variation (Figure 7). The resorbed cores have the most Mg rich, Ti-poor compositions, with Fe increasing slightly towards crystal margins. Micro-phenocrysts have the most Ca-rich compositions, similar to the rims of the megacrysts.

Olivine (Fo_{82} to Fo_{84}) in the nephelinite lavas tends to be euhedral, but is commonly altered to iron oxide and serpentine. Crystals range from 0.4mm to 3mm in size. The modal content is about 5% but variability is illustrated by one sample that had 10%.

Subhedral nepheline is present in rare patches (middle bottom, Figure 8) and the groundmass nepheline is usually altered. Acicular apatite is sometimes enclosed in pyroxene phenocrysts. Rare

Table 3. Mean composition and structural formulae (to 23 oxygen atoms) of sodic amphibole (magnesio-kataphorite) and kaersutite in the nephelinite of the Mashikiri Formation (classified after Richard and Clarke, 1987).

	1	2
SiO_2	51.15	42.40
TiO_2	1.00	4.55
Al_2O3	3.90	11.14
FeO	9.58	10.21
MnO	0.17	0.26
MgO	18.84	13.27
CaO	6.07	9.97
Na_2O	6.54	3.54
K_2O	1.64	0.90
Cl	nd	0.05
F	nd	0.17
Total	98.89	96.46
(Cl, F) ∫ O	nc	0.08
Total	98.89	96.38
Si	7.17	6.30
Al	0.65	1.70
$Fe^{3}+$	0.19	0.00
Σ T	8.00	8.00
Al	0.00	0.25
$Fe^{3}+$	0.72	0.07
Ti	0.11	0.51
Mg	3.94	2.94
$Fe^{2}+$	0.21	1.20
Mn	0.02	0.03
Σ C	5.00	5.00
Ca	0.91	1.59
Na	1.09	0.41
Σ B	2.00	2.00
Na	0.69	0.61
K	0.29	0.17
Σ A	0.98	0.78
Cl	0.00	0.01
F	0.00	0.08
Σ Cations	15.98	15.78

1. Magnesio-katophorite (3 analyses)
2. Kaersutite (5 analyses)

amphibole (pleochroic from yellow-green to pink) occurs both as a phenocryst phase and as an identifiable groundmass mineral in coarser-grained rocks. Sodic amphibole was previously also noted in nephelinites from the Pafuri region (Rogers, 1925; Lombaard, 1952, Bristow, 1980; 1984). The small amphibole phenocrysts in the lower parts of the Olifants River succession are kaersutite to magnesio-kataphorite (Table 3). The groundmass amphibole is associated with altered nepheline and rarely with biotite (altered to chlorite). Zircon crystals are often included in pyroxene megacrysts.

The opaque oxide phenocrysts are usually euhedral, never exceeding 1mm in size (Figures 8 and 9). Representative analyses are presented in Table 4. Exsolution lamellae are discernible and compositional

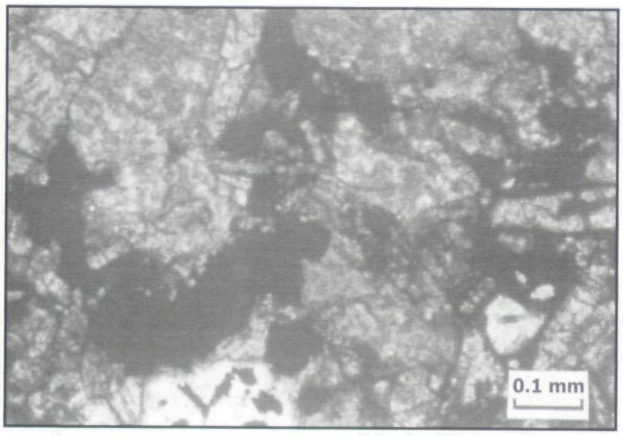

Figure 8. Coarse-grained nephelinite showing clinopyroxene macrophenocryst (cpx), euhedral nepheline (ne), anhedral amphibole (a) and euhedral opaque oxides (black).

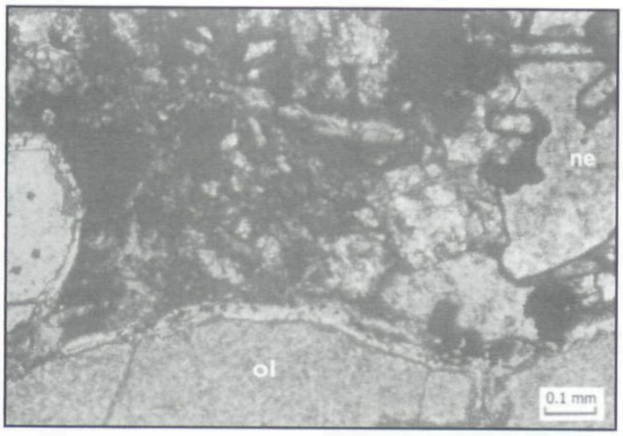

Figure 9. Nephelinite showing olivine phenocrysts (ol) with peripheral reaction rims consisting of serpentine, embayed nepheline phenocrysts (ne) and pyroxene laths in the groundmass that also contains euhedral opaque oxides.

variation in the magnetite/ulvospinel and hematite/ ilmenite solid solution series is limited.

Geochemistry

The whole rock major and trace element analyses were determined by XRF at the University of the Free State (using the method of Norrish and Hutton, 1969), and REE analyses were done at the University of Cape Town by ICP-MS (Table 5).

Major element variation and modelling

Major elements are plotted against MgO in Figure 10. The sample array for the Olifants River section is more extensive (6 to 11%) than the data for the Pafuri region (7 to 8.5%) previously published by Bristow (1984), but exhibits a similar restricted variation in major oxide composition. The one sample analysed for the Olifants River section by Bristow (KA16, 1984) is near the lower end of the array. Contents of the alkalis, Al_2O_3 and P_2O_5 are relatively high, while there is no discernible correlation between CaO and MgO. The distribution patterns suggest fractionation of MgO-rich phases (with

Table 4. Representative opaque oxide analyses from Mashikiri Formation nephelinites. Structural formulae calculated to 24 cations (Fe^{3+} stoichiometrically calculated using the MINFILE software of Afifi and Essene, 1988).

	1	2	3
SiO_2	0.96	0.96	2.64
TiO_2	28.23	9.40	3.86
Al_2O_3	0.31	0.32	0.76
Cr_2O_3	0.96	0.21	0.96
$FeO_{(T)}$	67.12	85.52	88.78
MnO	0.83	1.50	0.85
MgO	0.03	0.02	0.22
CaO	0.52	0.24	0.31
ZnO	0.14	0.16	0.05
Total	99.10	98.34	98.46
Si	0.28	0.28	0.76
Ti	6.30	2.07	0.84
Al	0.11	0.11	0.26
Cr	0.23	0.05	0.22
Fe^{3+}	2.49	11.13	12.31
Fe^{2+}	14.17	9.86	9.19
Mn	0.21	0.37	0.21
Mg	0.01	0.01	0.09
Ca	0.17	0.08	0.10
Zn	0.03	0.03	0.01

1. Titano-magnetite 2. Magnetite 3. Magnetite

minor contributions from SiO_2, TiO_2, Fe_2O_3 and MnO; Figure 10). Application of the methods of Cox et al. (1979), supply the following possible fractionation sequences: (i) cpx → ti-mt (ii) cpx → mt (iii) cpx → ti-mt +mt (iv) ol → cpx → ti-mt → mt (v) ol → cpx → ti-mt (vi) ol → cpx → mt. When the eigen vectors for all nephelinites calculated by Le Maitre (1976) are used, linear arrays are generated on binary plots. The first three eigen vectors collectively represent most of the variance (eigen values: 52% + 20% + 14%). The array for the Olifants River samples coincides with the near linear trend for ol + cpx fractionation, differing from that of the Pafuri region (Figure 11).

The variation can be explained by either nepheline or cpx and/or olivine fractionation. According to the crystallisation sequence model of Nathan and van Kirk (1978) the least fractionated sample (sample 1, Table 5) would sequentially yield ne-plag-mt-(leucite)-augite-ol-hy at 1 atmosphere. Nepheline would, however, be an early crystallising mineral only for magma representing the whole rock chemistry including the phenocrysts. When phenocrystal phases (olivine and pyroxene) are removed, the crystallisation sequence from the remaining melt would be plag-mt-ne-aug-(leucite)-hy-ol. This agrees with the observed matrix texture. The variation in chemical composition of the Olifants River sample suite can be explained by fractionation of cpx and ol at high pressure.

Models of fractional crystallisation of derived nephelinite lava from a primitive parent are displayed in Table 6. Evolved lava with the composition of sample 11

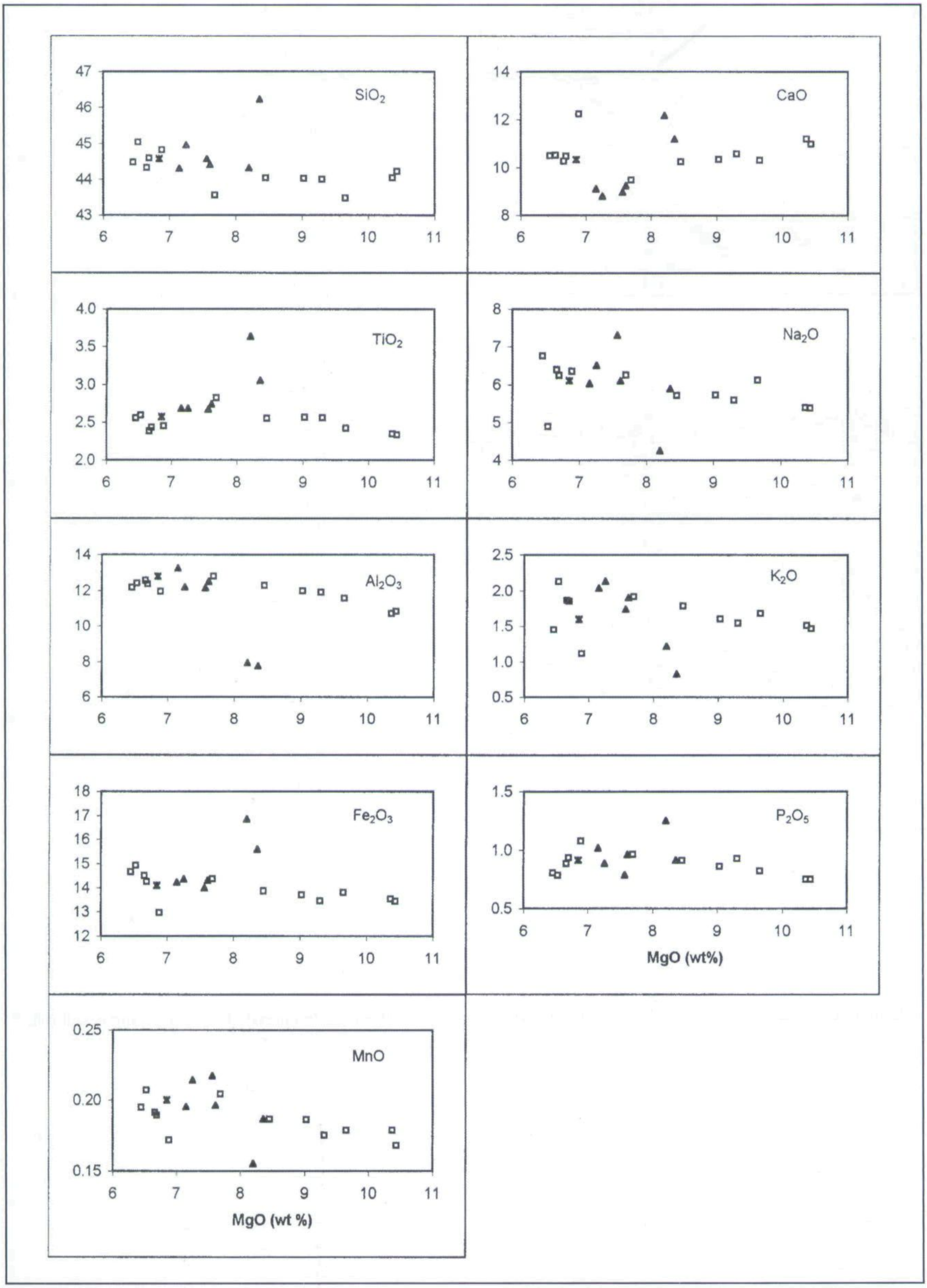

Figure 10. Analytical data for the chemically analysed nephelinite samples (Table 5) plotted as MgO against other oxides. Square symbols represent the new analyses provided in Table 5. Triangles are the samples analysed by Bristow (1984) from the Pafuri region, the single asterisk is the one sample from the Olifants River section given by Bristow (1984).

Table 5. Chemical composition of the Mashikiri Formation nephelinites occurring along the Olifants River of the Kruger National Park. Major elements in weigth per cent and trace elements in ppm (nd = not determined).

Sample	1	2	3	4	5	6	7	8	9	10	11	12	KA16	Mean	AV1	World
SiO_2	42.11	41.88	41.33	42.69	42.51	42.50	42.63	41.76	42.41	41.70	41.37	41.08	42.94	44.21	44.86	41.24
TiO_2	2.22	2.23	2.30	2.48	2.47	2.46	2.76	2.28	2.31	2.24	2.38	2.36	2.48	2.49	2.87	2.70
Al_2O_3	10.32	10.17	10.99	11.54	11.55	11.85	12.51	11.11	11.75	11.81	11.40	11.25	12.31	11.95	11.45	14.56
Fe_2O_3	12.79	12.86	13.12	13.05	13.23	13.37	14.05	12.08	13.55	13.64	13.70	13.53	13.57	13.94	14.52	13.20
MnO	0.16	0.17	0.17	0.17	0.18	0.18	0.20	0.16	0.18	0.18	0.19	0.18	0.19	0.19	0.19	0.26
MgO	9.94	9.86	9.18	9.03	8.72	8.16	7.53	6.42	6.37	6.27	6.00	5.96	6.60	8.20	7.51	6.49
CaO	10.47	10.66	9.89	10.25	9.99	9.88	9.27	11.41	9.97	9.66	9.66	9.69	9.96	10.59	10.20	12.08
Na_2O	5.12	5.13	5.81	5.42	5.53	5.51	6.12	5.92	5.93	6.01	4.49	6.24	5.88	5.89	5.86	4.87
K_2O	1.40	1.44	1.60	1.50	1.55	1.72	1.87	1.04	1.76	1.75	1.95	1.34	1.54	1.66	1.60	3.51
P_2O_5	0.71	0.71	0.78	0.90	0.83	0.88	0.94	1.00	0.89	0.83	0.72	0.74	0.88	0.87	0.93	1.09
H_2O-	0.10	0.11	0.18	0.38	0.30	0.40	0.21	0.60	0.30	0.48	0.62	0.31	0.09			
LOI	2.99	2.98	3.00	3.12	3.60	3.28	0.92	3.69	3.65	3.55	4.07	4.92	3.67			
Total	98.33	98.20	98.25	100.53	100.46	100.19	99.01	97.47	99.07	98.12	96.55	97.60	100.11			
Rb	47	51	63	53	59	55	53	37	59	52	89	64	39	60	49	
Ba	1089	1134	995	1026	1068	1268	1277	1417	1319	1626	1288	1443	1329	1312	1365	
Sr	1002	1025	1060	1002	1051	977	1334	1056	1164	946	1547	1190	1319	1172	1080	
Zr	102	103	109	118	115	120	157	104	96	104	78	90	112	114	166	
Nb	76	77	86	68	68	68	84	81	84	76	84	80	83	82	96	
Cr	434	448	365	313	283	220	95	66	71	67	63	66	59	219	93	
V	330	338	347	338	372	313	305	270	346	265	423	406	298	356	311	
Sc	25	20	17	13	18	16	17	24	21	15	14	14	14	19	18	
Ni	180	179	156	132	126	106	71	58	59	60	67	64	83	111	70	
Co	54	52	56	56	54	58	49	45	53	51	56	52	51	56	54	
Zn	109	110	110	110	113	114	110	119	115	121	123	128	116	121	127	
Cu	184	180	210	196	193	125	127	201	131	172	191	186	364	184	241	
Y	19	19	20	17	19	20	26	22	20	20	21	24	17	22	23	
Cs	2.04	nd	nd	nd	nd	nd	nd	nd	nd	nd	6.43	nd				
Th	1.75	nd	nd	nd	nd	nd	nd	nd	nd	nd	1.93	nd				
U	0.40	nd	nd	nd	nd	nd	nd	nd	nd	nd	0.34	nd				
Hf	3.37	nd	nd	nd	nd	nd	nd	nd	nd	nd	3.26	nd				
Ga	15.00	nd	nd	nd	nd	nd	nd	nd	nd	nd	19.00	nd				
Pb	10.10	nd	nd	nd	nd	nd	nd	nd	nd	nd	8.50	nd				
Ta	3.49	nd	nd	nd	nd	nd	nd	nd	nd	nd	3.90	nd				
La	21.54	nd	nd	nd	nd	nd	nd	nd	nd	nd	23.75	nd				
Ce	37.08	nd	nd	nd	nd	nd	nd	nd	nd	nd	40.06	nd				
Pr	4.32	nd	nd	nd	nd	nd	nd	nd	nd	nd	4.52	nd				
Nd	17.08	nd	nd	nd	nd	nd	nd	nd	nd	nd	17.69	nd				
Sm	3.62	nd	nd	nd	nd	nd	nd	nd	nd	nd	3.72	nd				
Eu	1.20	nd	nd	nd	nd	nd	nd	nd	nd	nd	1.24	nd				
Gd	3.18	nd	nd	nd	nd	nd	nd	nd	nd	nd	3.35	nd				
Tb	0.50	nd	nd	nd	nd	nd	nd	nd	nd	nd	0.52	nd				
Dy	2.82	nd	nd	nd	nd	nd	nd	nd	nd	nd	3.05	nd				
Ho	0.55	nd	nd	nd	nd	nd	nd	nd	nd	nd	0.60	nd				
Er	1.41	nd	nd	nd	nd	nd	nd	nd	nd	nd	1.62	nd				
Tm	0.20	nd	nd	nd	nd	nd	nd	nd	nd	nd	0.23	nd				
Yb	1.15	nd	nd	nd	nd	nd	nd	nd	nd	nd	1.42	nd				
Lu	0.18	nd	nd	nd	nd	nd	nd	nd	nd	nd	0.23	nd				

Samples 1 – 12 = new analyses, sample KA16 from Bristow (1984), Mean = mean from new analyses, AV1 = mean of Bristow (1984) including data from the Pafuri region (8 analyses). World = mean world nephelinite as calculated by Le Maitre (1976) from 176 analyses. All means calculated to 100% volatile free.

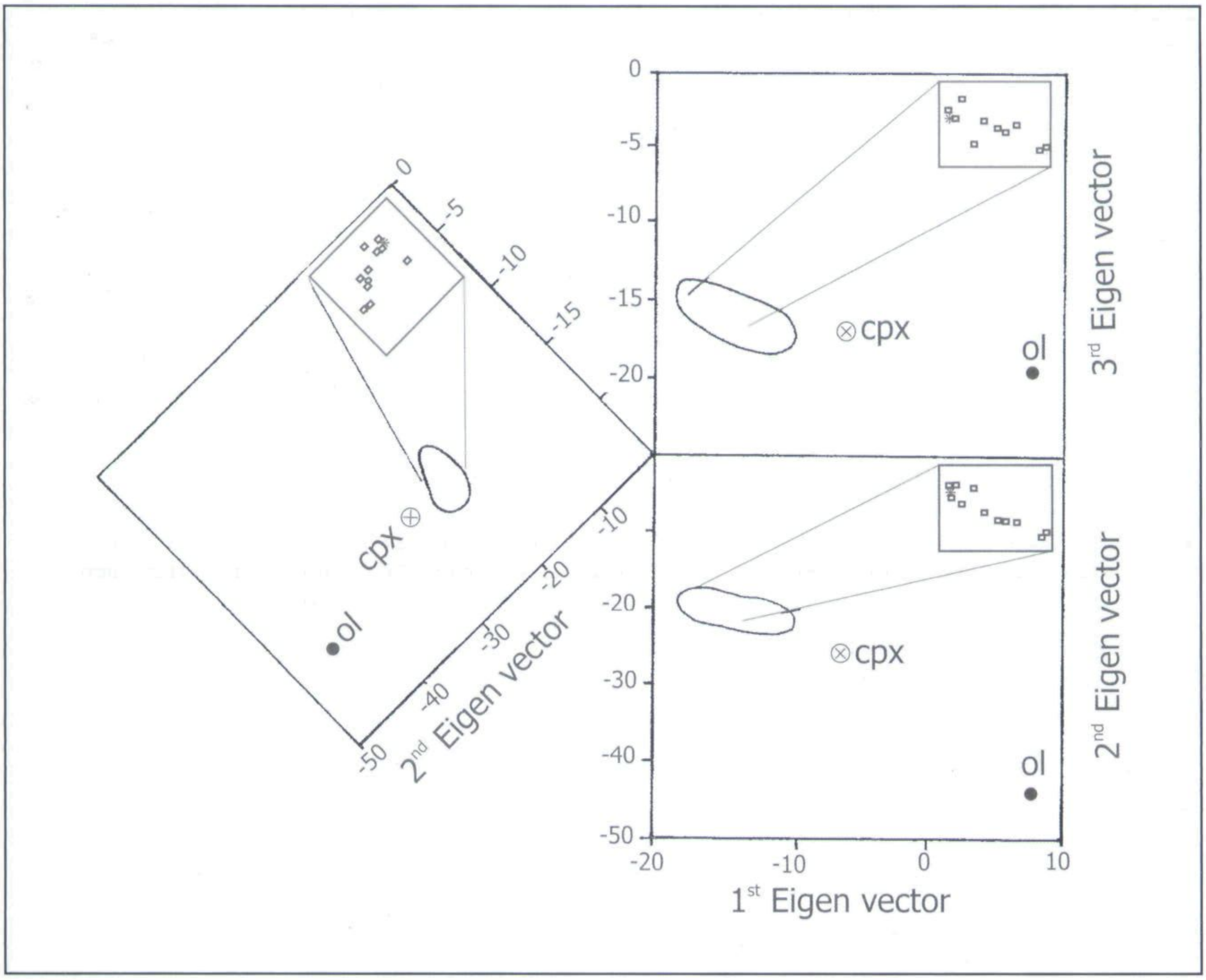

Figure 11. Analysed samples of nephelinites from the Mashikiri Formation, plotted along the eigen vector axes for all nephelinites calculated by Le Maitre (1976). The original axes represent eigen values of 52%, 20% and 14% respectively for the 1st, 2nd and 3rd eigen vectors so that a three dimensional diagram of the first three vectors represents the major part of the chemical variation. The diagram shows the positions of the rock-forming minerals olivine (ol) and clinopyroxene (cpx) and the outlined area represents the nephelinite analyses from the Olifants River section (Table 5) as well as the Pafuri and Sabi regions (Bristow (1984). In the enlarged insets the samples for the Olifants River section are distinguishable with a single asterisk for the sample given by Bristow (1984).

can be explained by 12.5% fractional crystallisation of a primitive liquid represented by sample 1. The separated phases are clinopyroxene (50%), olivine (29%) and nepheline (21%). A better D^2 value is produced, if titano-magnetite is included in the model (12.5% crystallisation: clinopyroxene 50%, olivine 16%, nepheline 27% and titano-magnetite 7% fractionation). The model of Bristow (1984) for the Pafuri and Sabi regions provided fractionation with very dominant clinopyroxene and with olivine only a minor third constituent.

Trace elements

Trace elements are plotted against MgO in Figure 12. The Nb/Ta peak (Figure 13) is similar to those of oceanic and continental alkali basalts, as well as P-MORB. This is unusual because continental flood basalts (CFB's) generally exhibit marked troughs, commonly attributed to an enriched mantle (Wilson, 1989). The positive anomalies for Sr and P could have been inherited from the magma source or derived from crustal contamination. The Ti peak may be attributed to either enrichment in titano-magnetite or ilmenite, or contamination with a Ti-enriched source. The negative Th and Zr anomalies probably represent early fractionation of zircon chadacrysts in pyroxene macro-phenocrysts. The flat overall REE pattern (Figure 14) is similar to that of other CFB's, with LREE enrichment (Wilson, 1989). A model of REE distribution as described in Rollinson (1995) using 12.5% Rayleigh fractionation of the mineral sequence determined above by major element least squares show very little difference between the measured and calculated samples (Table 7).

Discussion

The enrichment of incompatible minor and trace elements could be due either to magma derivation from an enriched source or to crustal contamination. Bristow (1984) concluded for the Pafuri region that fractionation

Table 6. Calculated least squares model for average nephelinite from the Mashikiri Formation. The calculation was done by aid of the MIXER programme (University of Cape Town) modified after the programme of Wright and Doherty (1970) using the method of Bryan *et al.* (1969).

	1	2	3	4	5	6
SiO_2	44.82	45.75	38.79	51.41	0.98	45.16
TiO_2	2.36	2.63	0.01	0.85	28.71	0.03
Al_2O_3	10.98	12.60	0.02	3.84	0.32	31.39
FeO*	12.25	13.62	16.30	6.99	68.28	0.54
MnO	0.17	0.21	0.29	0.10	0.85	0.01
MgO	10.58	6.63	44.21	13.49	0.31	0.01
CaO	11.14	10.68	0.26	22.11	0.53	0.72
Na_2O	5.45	4.96	0.09	1.17	0.01	17.44
K_2O	1.49	2.15	0.01	0.01	0.01	3.70
P_2O_5	0.76	0.80	0.01	0.01	0.01	0.01

1 = Primitive nephelinite composition (#1)
2 = Evolved nephelinite composition (#11)
3 = Average olivine
4 = Average cpx (excluding resorbed cores)
5 = Average titano-magnetite
6 = Average nepheline

	1	2
Sum of squares of differences	0.33%	1.10%
Olivine	8.70%	8.60%
Cpx	27.70%	14.60%
Nepheline	14.70%	6.00%
Ti-magnetite	3.80%	
Degree of crystallisation	12.50%	12.50%

	Obs	Calc-1	Diff-1	Calc-2	Diff-2
SiO_2	44.82	44.99	-0.07	45.97	-0.46
TiO_2	2.36	2.52	-0.16	1.99	0.37
Al_2O_3	10.98	11.44	-0.23	11.39	-0.20
FeO*	12.25	12.18	0.07	12.11	0.14
MnO	0.17	0.18	-0.01	0.19	-0.02
MgO	10.58	10.58	0.00	10.47	0.11
CaO	11.14	11.09	0.06	10.86	0.29
Na_2O	5.45	5.17	0.28	4.75	0.70
K_2O	1.49	1.53	-0.04	1.75	-0.26
P_2O_5	0.76	0.36	0.40	0.56	0.19

of cpx/ol took place at >30 kb. This was probably also the case for the Olifants River magma, but the chemical variation of the products (Table 5) are more tightly constrained than those from occurrences to the north (Pafuri region; Sabi region, Zimbabwe). The Olifants River sample suite also differs from the northern occurrences by the lack of evidence for crustal contamination, such as negative Nb/Ta anomalies. Compositional variation of the magmas under consideration was probably not influenced by crustal contamination. Bristow's (1984) conclusion that there may be two slightly different parental magmas coupled to different source regions should now be expanded to

Table 7. Calculated REE distribution of the Mashikiri nephelinites of the Olifants River section after 12.5% crystallisation of clinopyroxene (50%), olivine (29%) and nepheline (21%) from a primitive melt (Sample 1, Table 5) according to the method described by Rollinson (1995) to yield an evolved lava (Sample 11, Table 5). The data are normalised according to the values of Nakamura (1974) while the partition coefficients are from different sources (ol = Fuijimaki and Tatsumoto, 1984; cpx = McKenzie and O'Nions, 1991; ne = Larsen, 1979).

	1N	11N	12.50%	1	11	Calc
La	68.74	78.59	78.23	22.62	25.85	25.74
Ce	45.01	50.42	51.07	38.93	43.61	44.18
Pr	40.50	43.93	45.80	4.54	4.92	5.13
Nd	28.47	30.57	32.06	17.93	19.26	20.20
Sm	18.72	19.95	21.02	3.80	4.05	4.27
Eu	16.36	17.53	18.29	1.26	1.35	1.41
Gd	12.10	13.21	13.54	3.34	3.65	3.74
Tb	11.17	12.04	12.50	0.52	0.57	0.59
Dy	8.63	9.68	9.65	2.96	3.32	3.31
Ho	8.25	9.33	9.23	0.58	0.65	0.65
Er	6.58	7.84	7.37	1.48	1.76	1.66
Tm	7.00	8.35	7.84	0.21	0.25	0.24
Yb	5.49	7.03	6.14	1.21	1.55	1.35
				99.38	110.79	112.44

three members. The Olifants River section seems to be the least contaminated and most alkalic representative of the original partial melts from the mantle. Thompson *et al.* (1984) and Pearce (1983) respectively use the La/Nb and Th/Yb ratios to provide a measure of crustal contamination. In the case of the Mashikiri nephelinites, the calculated ratios once again indicate negligible contamination. The nephelinites plot in the Enriched Mantle Source field of Pearce's Ta/Yb vs. Th/Yb diagram, suggesting that they were derived from a single fertile mantle source. A single mantle source component provides an acceptable model (Figure 15). The Cr/Ni ratio of the most primitive sample indicates that this source had a peridotitic mineralogy. Garnet is almost certainly present according to the REE data, along with a phase responsible for releasing MREE, such as phlogopite.

Bristow *et al.* (1984) reports Sr isotope data for the Mashikiri nephelinites, with $^{87}Sr/^{86}Sr$ initial ratios for the Sabi-Lebombo region, ranging from 0.70510 to 0.70687. The one sample from the Olifants River Section yielded an initial ratio of 0.70520. This variation is attributed to derivation of the nephelinites from a source displaying Sr heterogeneity (Bristow, 1980; 1984), confirming the identification of at least three source regions mentioned above.

Frey *et al.* (1978) suggest that undersaturated magmas can be produced from lherzolitic mantle by small degrees of partial melting, if the source is first enriched in incompatible elements. The early high-pressure fractionation must have occurred after initial melting and melt segregation, but prior to ascent of the liquid. Ascent to shallower crustal levels was constrained

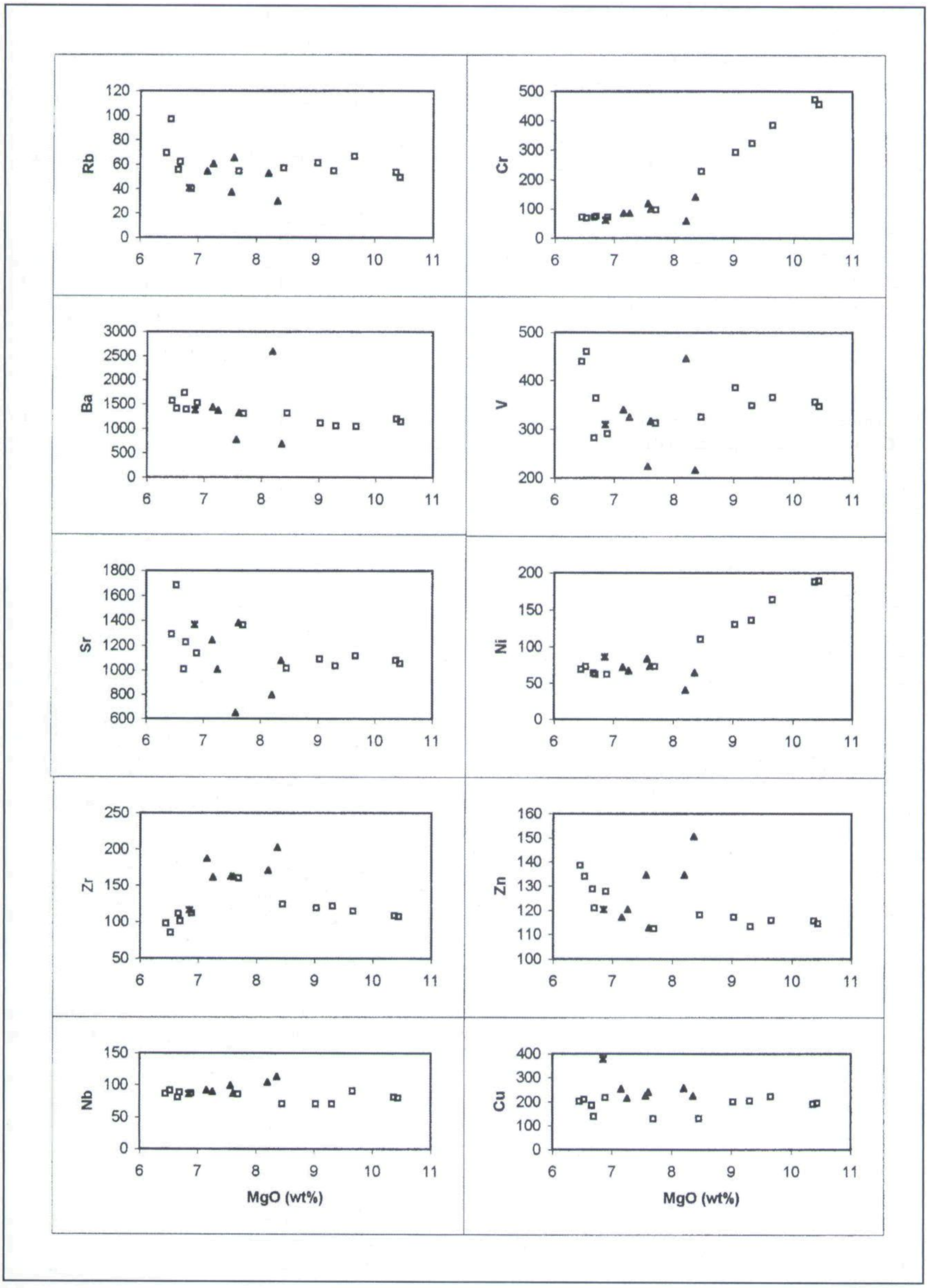

Figure 12. Analytical data for the chemically analysed nephelinite samples (Table 5) plotted as MgO against trace elements. Square symbols represent the new analyses provided in Table 5. Triangles are the samples analysed by Bristow (1984) from the Pafuri region; the single asterisk is the one sample from the Olifants River section given by Bristow (1984).

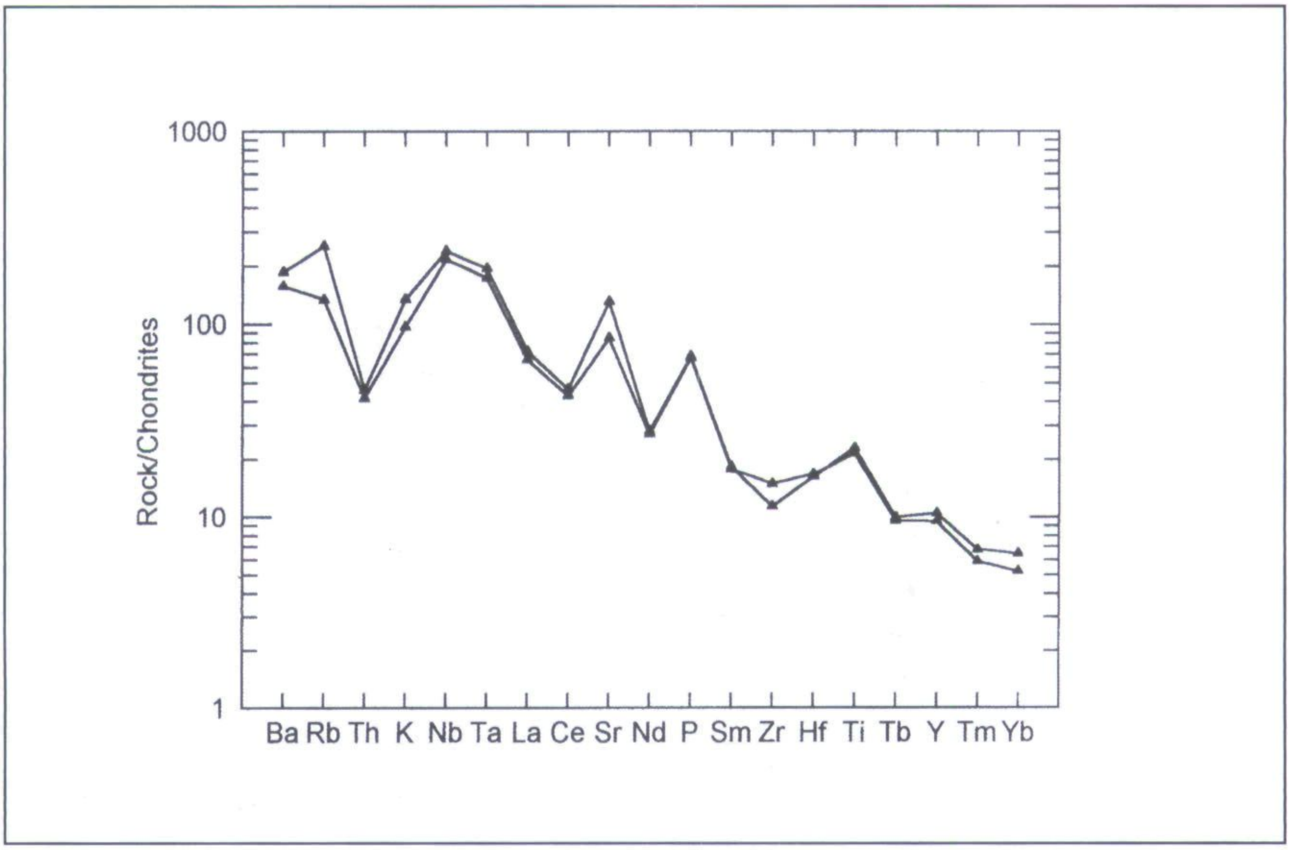

Figure 13. Chemical variation of the Mashikiri Formation nephelinites (supplied in Table 5) normalised against chondrite (Thompson, 1982).

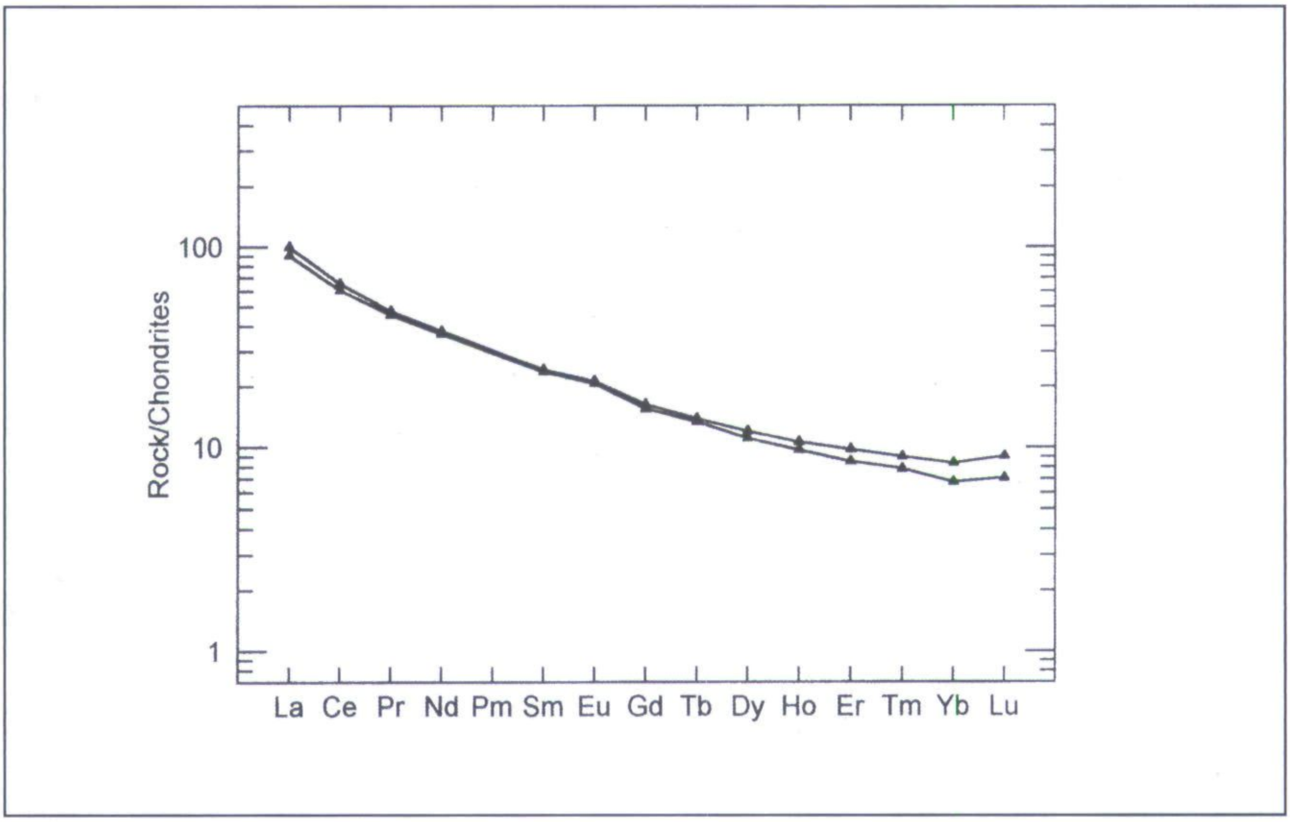

Figure 14. REE variation in the Mashikiri Formation nephelinites (supplied in Table 5) normalised against the chondrite of Sun and McDonough (1989)

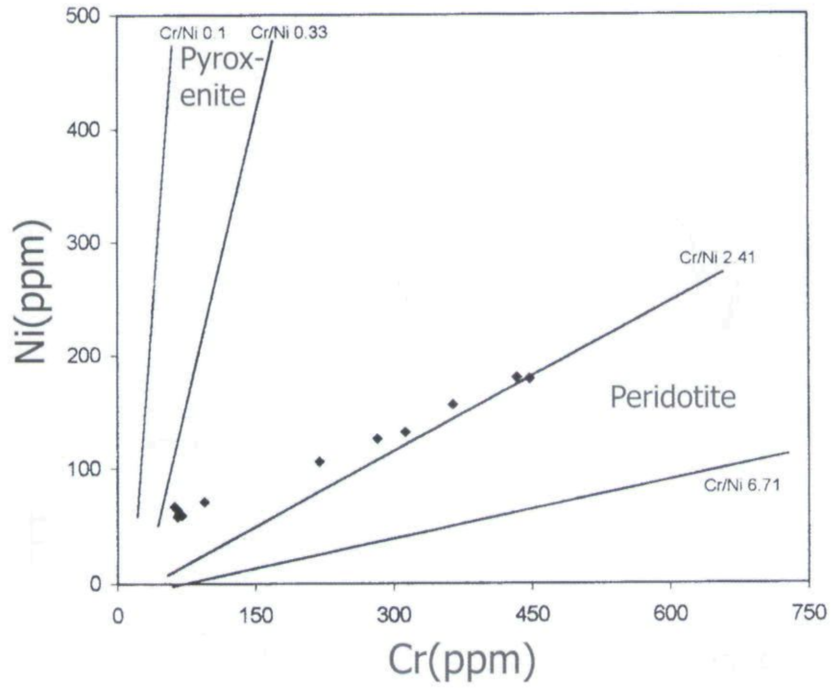

Figure 15. Distribution of Cr vs. Ni for the Mashikiri nephelinites (filled diamonds). The mantle lithology fields are indicated using the Cr/Ni ratios of liquids generated from garnet-peridotite and pyroxenite (after Leeman, 1976).

by the density of the magma and further ascent occurred only after a sufficient amount of early fractionation. The ascent to shallow crustal levels must have been relatively fast, as indicated by the closely spaced, multiple zoning of pyroxenes that indicate growth in a rapidly changing environment. This quick ascent caused second generation pyroxenes to crystallise as new crystals and overgrowths on first generation crystals. A quick ascent could also explain the lack of crustal contamination.

The nephelinite liquid was the first magma of any great volume in the Karoo volcanic event to penetrate the crust. The crustal rocks are therefore likely to have been relatively cool. This would encourage the development of a lining of solidified magma in transport fissures. Subsequent rising liquid using the same conduits would therefore be relatively isolated from the crustal rocks preventing contamination. Low-pressure fractionation could have taken place in ponded magma, accounting for the suite of lavas seen in outcrop, with relatively Fe-rich clinopyroxene (the third generation of pyroxenes), olivine and a Fe-Ti oxide in the matrix.

Acknowledgements

The authors would like to thank the Director of the KNP for permission to work in the Park and the staff for valued advice and assistance. We thank Dr. Freek Venter who was instrumental in getting the necessary permission and Mr. Arrie Schreiber for his help during the fieldwork. We would also like to thank Billiton and the FRD for financing the research and the University of the Free State for the use of their facilities. The authors wish to express their appreciation for the constructive reviews of the referees J.S. Marsh and M. Cloete.

References

Afifi, A.M. and Essene, E.J. (1988). MINFILE computer programme for calculating structural formulae of minerals from chemical analyses. *University of Michigan, Ann Arbor, Michigan, United States of America*.

Allsopp, H.L., Manton, W.I., Bristow, J.W. and Erlank, A.J. (1984). Rb-Sr geochronology of Karoo felsic volcanics, *Geological Society of South Africa Special Publication*, **13**, 273-280.

Barton, J.M., Bristow, J.W. and Venter, F.J. (1986). A summary of the Precambrian granitoid rocks of the Kruger National Park. *Koedoe*, **29**, 39-44.

Bristow, J.W. (1980). *The geochronology and geochemistry of Karoo volcanics in the Lebombo and adjacent areas*. Unpublished PhD thesis, University of Cape Town, Cape Town, South Africa, 256pp.

Bristow, J.W. (1984). Nephelinites of the north Lebombo and south-east Zimbabwe, *Geological Society of South Africa Special Publication*, **13**, 87-104.

Bristow, J.W. and Venter, F.J. (1986). Notes on the Permian to Recent geology of the Kruger National Park. *Koedoe*, **29**, 117-124.

Bristow, J.W., Allsopp, H.L, Erlank, A.J., Marsh, J.S. and Armstrong, R.A. (1984). Strontium isotope characterization of Karoo volcanic rocks, *Geological Society of South Africa Special Publication*, **13**, 295-329.

Bryan, W.B., Finger, L.W. and Chayes, F. (1969). Estimating proportions in petrologic mixing equations by least squares approximation. *Science*, **163**, 926-927.

Cleverly, R.W. and Bristow, J.W. (1979). Revised volcanic stratigraphy of the Lebombo monocline. *Transactions of the Geological Society of South Africa*, **82**, 227-230.

Coffin, M.A. and Eldholm, O. (1994). Large Igneous Provinces: Crustal structure, dimensions and external consequences. *Reviews of Geophysics*, **32**, 1-36.

Cox, K.G. (1978a). Flood basalts, subduction and the break-up of Gondwanaland. *Nature*, 274, 47-49.

Cox, K.G. (1978b). Komatiites and other high-magnesia lavas; some problems. Philosophical Transactions of the Royal Society of London, **A 288,** 599-609.

Cox, K.G. (1980). A model for flood basalt volcanism. *Journal of Petrology,* **21**, 629-650.

Cox, K.G., Bell, J.D. and Pankhurst, R.J. (1979). The interpretation of igneous rocks. *Chapham and Hall, London, U.K.*, 450 pp.

Cox, K.G., Macdonald, R. and Hornung, G. (1967). Geochemical and petrographic provinces in the Karoo basalts of southern Africa. *American Mineralogist*, **52**, 1451-1474.

Duncan, R.A., Hooper, P.R., Rehacek, J., Marsh, J.S. and Duncan, A.R. (1997). The timing and duration of the Karoo igneous event, southern Gondwana. *Journal of Geophysical Research, Solid Earth Section*, **102**, 18127-18138.

Eales, H.V., Marsh, J.S. and Cox., K.G. (1984). The Karoo Igneous Province: An introduction, *Geological Society of South Africa Special Publication*, **13**, 1-26.

Frey, F.A., Green, D.H. and Roy, S.D. (1978). Integrated models of basalt petrogenesis: a study of quartz tholeiites to olivine melilitites from south eastern Australia utilizing geochemical and experimental petrological data. *Journal of Petrology*, **19**, 463-513.

Fuijimaki, H. and Tatsumoto, M. (1984). Partitions coefficients of Hf, Zr and REE between phenocrysts and groundmass. *Journal of Geophysical Research*, **89**, 662-672.

Henthorn, D.I. (1981). The magnetostratigraphy of the Lebombo Group along the Olifants River, Kruger National Park. *Annals of the Geological Survey of South Africa*, **15/2**, 1-10.

Jantsky, J.G. (1980). Intrusives of Randian Age, *In*: L. E. Kent (Compiler), Lithostratigraphy of the Republic of South Africa, South West Africa/Namibia and the Republics of Bophuthatswana, Transkei and Venda, *Geological Survey of South Africa Handbook*, **8**, 181-183.

Larsen, L.M. (1979). Distribution of REE and other trace elements between phenocrysts and peralkaline undersaturated magmas, exemplified by rocks from the Gardar igneous province, south Greenland. *Lithos*, **12**, 303-315.

Lombaard, B.V. (1952). Karroo dolerites and lavas. *Transactions of the Geological Society of South Africa*, **55**, 175-198.

Leeman, W.P. (1976). Petrogenesis of the McKinney (Snake River) olivine tholeiite in the light of Rare-earth element and Cr/Ni distributions. *Geological Society of America Bulletin*, **87**, 1582-1586.

Le Maitre, R.W. (1976). The chemical variability of some common igneous rocks. *Journal of Petrology*, **17**, 589-637.

McKenzie, D. and O'Nions, R.K. (1991). Partial melt distributions from inversion of rare Earth element concentrations. *Journal of Petrology*, **32**, 1021-1091.

Nakamura, N. (1974). Determination of REE, Ba, Fe, Mg, Na and K in carbonaceous and ordinary chondrites. *Geochimica et Cosmochimica Acta*, **38**, 757-775.

Nathan, H.D. and Van Kirk, C.K. (1978). A model for magmatic crystallization. *Journal of Petrology*, **19(1)**, 66-94.

Norrish, K. and Hutton, J.T. (1969). An accurate X-ray spectrographic method for the analysis of a wide range of geological samples. *Geochimica et Cosmochimica Acta*, **33**, 431-453.

Pearce, J.A. (1983). Trace element characteristics of lavas from destructive plate boundaries, In: R. S. Thorpe (Editor), Andesites. *John Wiley and Sons, New York, U.S.A.*, 525-548.

Rhodes, R.C. and Krohn, D.H. (1972). Tectonic control over geochemical variation in the Karoo basaltic province of southern Africa. *Transactions of the Geological Society of South Africa*, **75**, 11-21.

Richard, L.R. and Clarke, D.B. (1987). AMPHIBOL: Computer software for calculating structural formulae and classifying amphiboles. *Department of Geology, Dalhousie University, Halifax, Canada*.

Rogers, A.W. (1926). Notes on the North-eastern part of the Zoutpansberg District. *Transactions of the Geological Society of South Africa*, **28**, 33-53.

Rollinson, H.R. (1995). Using geochemical data: evaluation, presentation, interpretation. *Longman Group, London, U.K.*, 352 pp.

Schutte, I.C. (1986). The general geology of the Kruger National Park. *Koedoe*, **29** , 13-38.

Sun, S.S. and McDonough, W.F. (1989). Chemical and isotopic systematics of oceanic basalts: implications for mantle composition and processes,. *In*: A. D. Saunders and M. J. Norry (Editors), Magmatism in ocean basins, *Geological Society of London, Special Publication*, **42**, 313-345.

Thompson, R.N. (1982). British Tertiary volcanic province. *Scottish Journal of Geology*, **18**, 49-07.

Thompson, R.N., Morrison, M.A., Hendry, G.L. and Parry, S.J. (1984). An assessment of the relative roles of crust and mantle in magma genesis: an elemental approach. *Philosophical Transactions of the Royal Society of London*, **A310,** 549-90.

White, R.S. and McKenzie, D. (1995). Mantle plumes and flood basalts. *Journal of Geophysical Research*, **100,** 17543-17585.

Wilson, M. (1989). Igneous petrogenesis: a global tectonic approach. *Chapman and Hall, London, U. K.*, 466 pp.

Wright, T.L. and Doherty, P.C. (1970). A linear programming and least squares computer method of solving petrological mixing problems. *Geological Society of America Bulletin*, **81**, 1995-2008.

Editorial handling: J. M. Barton Jr.